Astron. Astrophys. 325, 803–812 (1997)

ASTRONOMY
AND
ASTROPHYSICS

Emission of hydrogen lines by moving solar prominences

C. Gontikakis, J.-C. Vial, and P. Gouttebroze

Institut d'Astrophysique Spatiale, Unité mixte CNRS-Université Paris XI, Bâtiment 121, F-91405 Orsay Cedex, France

Received 19 November 1996 / Accepted 24 March 1997

Abstract. We study the radiative transfer processes occurring in a plane-parallel slab standing vertically above the chromosphere and moving upward as a solid body. This structure simulates a prominence in the phase of eruption or a quiescent prominence where the plasma presents bulk velocities. We use partial redistribution for the description of the resonance scattering in the hydrogen Lα and Lβ lines. We compute the Lα, Lβ and Hα emergent line profiles of hydrogen for different velocities. We derive the variation of the emitted intensities as a function of the velocity for various temperatures and thicknesses. We discuss our results in view of the diagnostic of erupting prominences in Lyman lines that SOHO observations can provide.

Key words: radiative transfer – prominences – radial velocities

1. Introduction

Prominences are cold and dense plasma structures embedded in the hot and tenuous corona. Their lifetime varies from hours to months and they disappear in different ways. In the case where the prominence erupts, the structure as a whole is ejected out of the Sun. The material acquires bulk velocities of the order of several hundreds km s^{-1} (Tandberg-Hanssen 1995). In active prominences, we observe motions of the magnetically confined material of the order of a few tens km s^{-1}. The dynamic activity in prominences is transient which makes the diagnostic quite difficult.

The attempts of diagnostic of prominence in a transient state have been based until now on Hα and white light measurements. These data are not the best ones for deriving the temperature of the structure. A promising diagnostic method is based on the spectral analysis of the strong and optically thick lines of hydrogen.

We know from Hirayama (1963) that the radiative transfer in solar prominences is essentially governed by the scattering of the photospheric and chromospheric light which illuminates the structures. When the prominence moves, its illumination is Doppler shifted and the emergent intensity varies as a function of the velocity. This effect was first considered by Rompolt (1967a, b; 1969). Hyder and Lites (1970) applied it to the variation of the Hα radiation emitted by an eruptive prominence.

The first computation of a static prominence treating the radiative transfer in non-LTE using partial frequency redistribution (PRD) for the scattering in the Lα and Lβ lines and complete redistribution (CRD) for Hα, were performed by Milkey et al. (1978), Heinzel et al. (1987) (hereafter HGV) and Gouttebroze et al. (1993) (hereafter GHV). GHV computed the emergent hydrogen line profiles for a grid of 140 models with different values for the temperature, the geometrical width and the pressure. Among other they found that the correlation between the Hα total intensity and the emission measure can be used to diagnose the electron density or the width of the structure along the line of sight (see also Heinzel et al. 1996). They also confirmed that the slope of the Lyman continuum is a good indicator of the electron temperature.

Heinzel and Rompolt (1987) (hereafter HR) were the first to elaborate a non-LTE calculation of the radiative transfer inside a prominence, taking into account the effect of radial velocities. In their model, Lα and Lβ are optically thick and Hα is optically thin. They used CRD for the three lines, and computed the intensity integrated over frequency as a function of the velocity.

Gontikakis et al. (1996) (hereafter GVG) developed similar calculations as HR but using PRD for Lα and Lβ lines. They compared the total intensities of the Lα, Lβ and Hα lines calculated in CRD and PRD, as a function of velocity. They found that CRD can be a good approximation for computing the Lα integrated intensity but not for the Lβ and Hα intensities.

In this work, we continue the effort of GVG with the study of the *profiles* of these lines. The line profiles carry much more information about the temperature and the velocity than the integrated intensities do and they can be used as a strong diagnostic tool.

In the next section we describe the numerical procedure used in our calculations. Section 3 shows a comparison of the velocity effect on the line profiles when PRD and CRD are used. In section 4 we present the influence of the prominence model (taking different temperatures, widths and pressures) on the signature of the velocity effects. Section 5 compares the correlations between the emission measure and Hα intensity

Send offprint requests to: J.-C. Vial

with and without radial velocity. Finally we discuss the way we can use these results for the diagnostic of erupting prominences.

2. The numerical procedure

We use the IAS code ("HYDR"), modified in order to take into account the Doppler shift due to the radial velocity. This code solves the equations of pressure, ionization and statistical equilibrium of the hydrogen atom and radiative transfer in lines and continua. It uses the equivalent-two-level-atom technique and the solution of the statistical equilibrium is achieved by iteration. The radiative transfer equation is solved by the Feautrier method with variable Eddington factors (Auer and Mihalas 1970). The prominence is represented by a plane-parallel slab illuminated on both sides by the incident photospheric and chromospheric radiations. The slab, isothermal and isobaric, is perpendicular to the Sun surface. The plasma is composed by neutral and ionized hydrogen and neutral helium; the helium abundance is equal to 0.1. The incident radiation is expressed by the mean intensity:

$$J_0(\nu) = \frac{1}{4\pi} \oint I_0 \left(\nu + \frac{\nu_0}{c} \mathbf{V} \cdot \mathbf{n}', \mathbf{n}' \right) d\mathbf{n}', \quad (1)$$

where $I_0(\nu, \mathbf{n})$ is the specific intensity of the incident radiation, ($\mathbf{n}'$ is the direction vector, ν is the frequency) and $\mathbf{V}$ the outward radial velocity. The incident profiles are not only shifted but their shape also changes with velocity as the result of averaging in Eq. (1). In Fig. 1 we see that the profile of the mean Lα intensity loses its characteristic double peak structure at high velocities. As we cannot use any symmetry, we take full profiles for the incident lines and at all the steps of our calculation. For the incident intensity we use the Lyman lines recorded by OSO-8 (Vial 1982), the Balmer limb-darkened profiles of David (1961), and the Paschen and Brackett profiles from Zelenka (1976). The line profiles have been adjusted to the continuum levels by using polynomial expansions (Pierce and Slaughter 1977; Pierce et al. 1977). We extrapolate the observed Lα and Lβ profiles beyond 2 Å using a Lorentz fit function.

As input parameters we use the electron temperature T, the gas pressure P, the width D of the slab, the altitude H above the chromosphere and the macroscopic velocity V. The turbulent velocity is neglected. The values that we choose for the physical parameters are close to the average values given by observations. For the temperature we take 4300 K, 8 000 K and 15 000 K. The pressure takes the values of 0.01, 0.1 and 1 dyn cm^{-2} and the altitude is taken as 10 000 km. We use the following values for the macroscopic velocity of the structure: 0, 40, 80, 120, 200 and 400 km s^{-1}.

3. Comparison between CRD and PRD

The partial redistribution (PRD) is a more accurate way than the complete redistribution (CRD) for the treatment of the resonance scattering in Lα and Lβ lines in solar prominences, as demonstrated by Heinzel et al. (1987) (hereafter HGV). However, we also calculate the CRD case because its comparison to PRD raises interesting physical issues. GVG already found

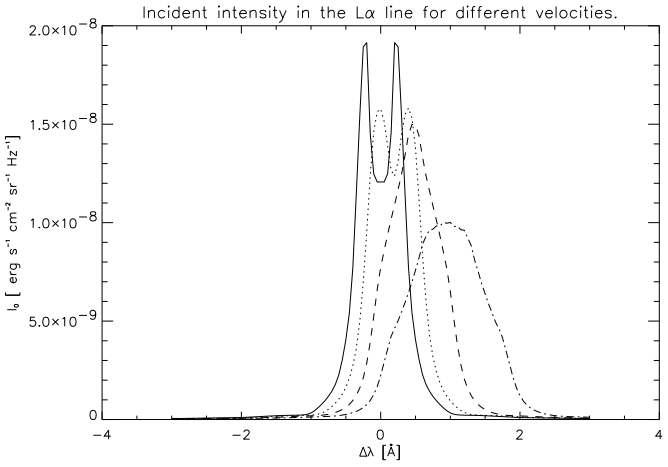

Fig. 1. Angle-averaged incident profiles of the Lα line at 10 000 km above the Sun. The full line is for zero velocity, the dots for 80 km s^{-1}, the dashes for 200 km s^{-1}, and the dot-dashes for 400 km s^{-1}. We see the disappearance of the double peak of the incident line profile with the growth of velocity (photons coming from different parts of the surface are differently Doppler shifted).

that the relative intensities of Lα, Lβ and Hα as a function of velocity have approximately the same variations when they are calculated with the two redistributions (see GVG). Here, the relative intensity as a function of the velocity is the ratio of the intensity for a given velocity to the intensity for zero velocity.

Previous results can be summarized as follows. For PRD and CRD, Lα presents a Doppler dimming because the incident line is in emission. Hα shows a brightening increase for velocities up to 160 km s^{-1} followed by a decrease at higher velocities. Lβ has the same dependence with the velocity as Hα, but the maximum brightening is at 80 km s^{-1}.

At high velocities the Hα intensity decreases because the Lα dimming results in a decrease of level 2 population. The Lβ behaviour results from the decrease of resonance scattering since it is an emission line.

In PRD, as the Lα photons are scattered far inside the prominence body, as shown by HGV for zero velocity, the populations of levels two and three are enhanced in PRD. Consequently the intensities of Lα, Lβ and Hα are higher in PRD than in CRD for all the values of the velocities (see GVG, Fig. 3c and 3d for Lα and Hα absolute intensities). Also as the level two is more populated in PRD, the incident Balmer continuum is more efficient and the plasma is more ionized (Fig. 3a and 3b in GVG).

For a given prominence model (T = 8 000 K, D = 2 000 km, P = 0.1 dyn cm^{-2} and H = 10 000 km), we calculate the emergent Lα, Lβ and Hα lines for the PRD and CRD cases. In Fig. 2 we present the results of these calculations for four values of the velocity and we see that the PRD profiles have different features than the CRD ones. In order to understand these differences we have to consider the redistribution effects combined with the radiative transfer.

The redistribution function may be divided into three domains according to the value of x, the frequency of the incident

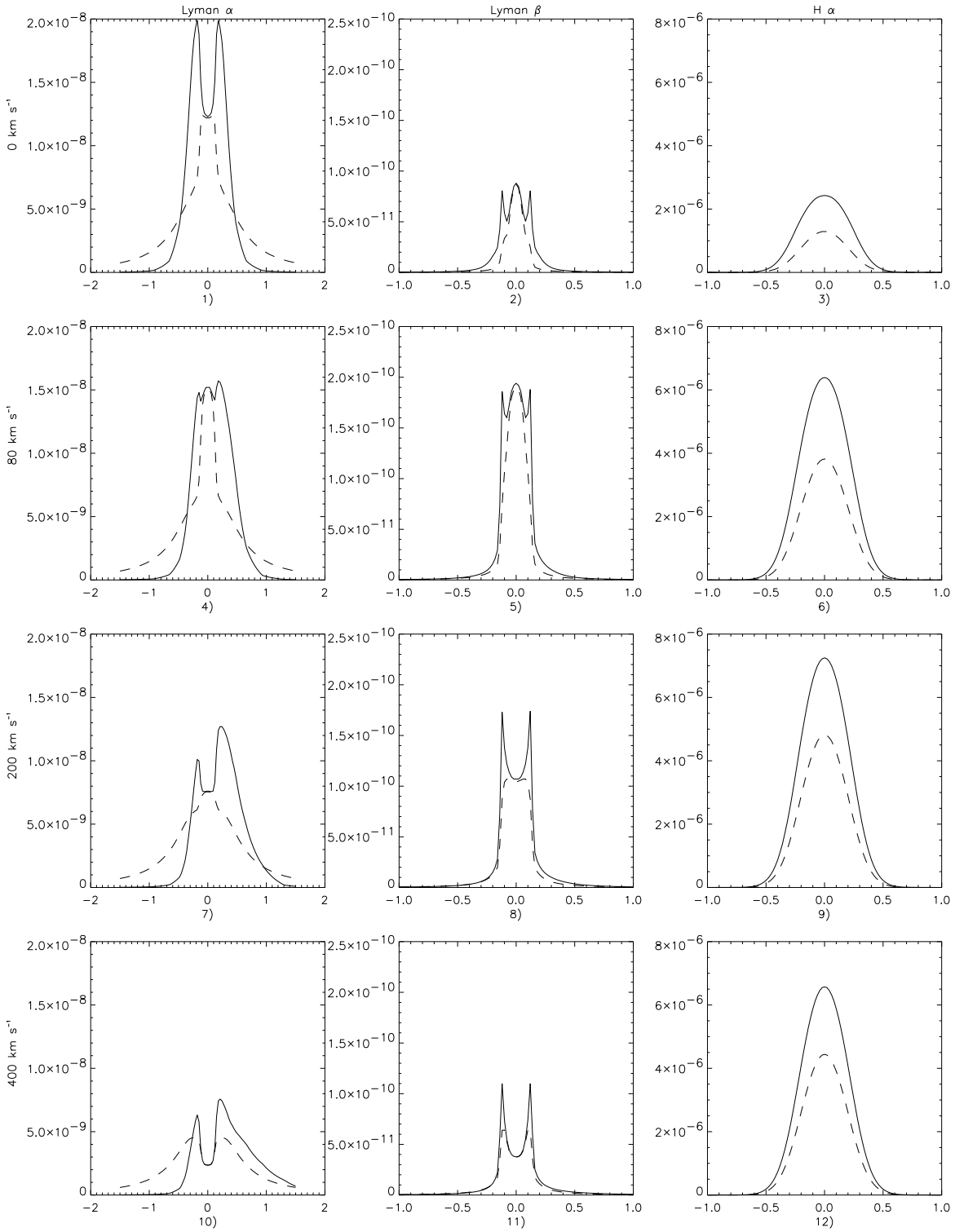

Fig. 2. The profiles of Lα, Lβ and Hα (columns 1, 2, 3) for four velocities :0, 80, 200 and 400 km s^{-1} (rows 1, 2, 3 and 4). The model has a temperature of 8 000 K, a thickness of 2 000 km and a pressure of 0.1 dyn cm^{-2}. PRD corresponds to the solid line and CRD to the dashed line. The intensity is in erg s^{-1}cm^{-2}sr^{-1}Hz^{-1} and the abscissa is in Å.

photon (in Doppler units). When $x < 3$, the emission comes principally from atoms absorbing near line center due to the Maxwellian distribution of velocities. The distribution of the emergent photons is Doppler-shaped, the scattering process is incoherent. When $x > 4$ the distribution of x', the frequency of the emergent photons, is roughly symmetric around $x' = x$ and we have quasi-coherent scattering. In the region $3 < x < 4$ the distribution of x' is in transition between the Doppler distribution and the coherent one (Hummer 1962).

Due to the non coherence of the redistribution functions for $x < 3$, CRD and PRD profiles yield comparable intensities inside three Doppler widths, which corresponds to 0.14 Å for Lα and 0.12 Å for Lβ, for all velocities (Fig. 2, columns 1 and 2).

In the Lα line the characteristic difference between the two cases of redistribution is the presence of peaks in the PRD emergent profile. For zero velocity the peaks represent a quasi-reproduction of the incident profile (HGV and Fig. 2.1). With the increase of velocity, the emergent profile shows a more intense peak on the red side of the profile and a lower one on the blue side for this line (Fig. 2.4, 2.7 and 2.10).

As the velocity increases the incident profile is shifted to the red. The major part of the incident photons will scatter in the red part of the line in a coherent way, and a small part of them will be scattered in the blue wing following the PRD function for:$3 < x < 4$ and $x > 4$. This results in the increase of asymmetry and reversal of the profiles in Fig. 2.4, 2.7, 2.10.

CRD redistributes the Lα photons into a Voigt-shaped, always symmetric profile. The result is that in the near wings, where we have the intense incident peaks, the CRD intensity is lower than the PRD, whereas in the far wings, where the incident light is faint, CRD is stronger than PRD (Fig. 2.1, 2.4, 2.7). At 400 km s^{-1} the incident peak is shifted to the far red wing and there, the PRD far red wing is stronger than the CRD one (Fig. 2.10). Finally, we present in Fig. 3 the incident Lα profile for v = 200 km s^{-1} and the emergent one corresponding to PRD calculation for a model with 8 000 K, 0.1 dyn cm^{-2} and a thickness of 2 000 km. We notice the equality between the two intensities at line center.

The Lβ line shows different features than Lα (Fig. 2, the second column). Two peaks are also present for all velocities, but they are always symmetric. Asymmetries due to the Doppler shift of the incoming radiation are visible at $\Delta\lambda \simeq 0.2$ Å and they are much smaller than in Lα. For Lα the only radiative process is the resonance scattering which is partially coherent. On the contrary, the spontaneous emission of Lβ photons from the level three populated by Hα is an incoherent process that is added to the quasi-coherent resonance scattering. The incident Hα is a very strong line (even if in absorption), and the incident photons penetrate deep inside the slab because the optical thickness of this line is $\tau_{H_\alpha} \simeq 1$ (contrary to the Lβ for which the medium is optically thick). Consequently the process of quasi-coherent scattering is dominated by other emission processes so that the Lβ profiles asymmetries are very small.

The Hα line is treated in CRD. The two types of Hα profiles (corresponding to a treatment of Lyman lines in PRD or in CRD) are quasi Doppler-shaped because of the small opacity of this transition; we notice the higher intensities in PRD due to the higher population of level 2. It should be pointed out that PRD/CRD behaviour is model-dependent (see e.g. Fig. 3 of GVG).

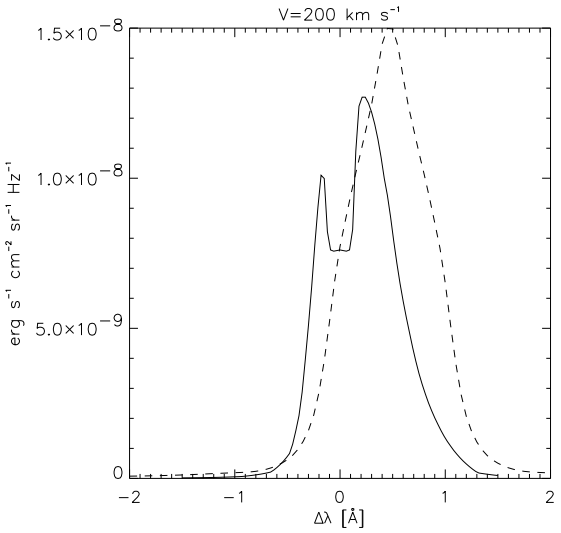

Fig. 3. Comparison between the mean incident (dotted line) and emergent (full line) profiles for the Lα line. The velocity is v = 200 km s^{-1}. The emergent profile is calculated in PRD. The prominence model is the same as the one used in Fig. 2.

Table 1. Dependence of the Lyman lines on the temperature (v = 200 km s^{-1}).

Temperature (K)	$\tau(L\alpha)$	I_{max}(Lα)	$I_{\Delta\lambda=1\text{Å}}$ (Lα)
4300	1.7×10^6	1.2×10^{-8}	3.5×10^{-9}
8 000	4.0×10^5	1.3×10^{-8}	1.4×10^{-9}
15 000	9008	2.5×10^{-7}	5.5×10^{-11}
Temperature (K)	$\tau(L\beta)$	I_{max}(Lβ)	$I_{\Delta\lambda=1\text{Å}}$ (Lβ)
4300	2.8×10^5	1.2×10^{-10}	7.2×10^{-12}
8 000	6.4×10^4	1.7×10^{-10}	3.6×10^{-12}
15 000	1445	3.2×10^{-9}	1.2×10^{-12}

4. The influence of the physical parameters

The velocity signature on the line profiles depends on the thermodynamic conditions and geometry of the model. Here we use three temperature values, (4300, 8 000 and 15 000 K) and three thicknesses (200, 2 000 and 10 000 km). The velocity goes up to 400 km s^{-1}.

For a temperature of 4300 K and a thickness of 2 000 km the Lα line shows a strong emission in the core of the line and a small peak in the red wing, when the velocity varies from 40 to 120 km s^{-1} (Fig. 4.4, 4.7, 4.10). For 40 km s^{-1} we also see a triple peak feature. We can interpret it as follows:because of

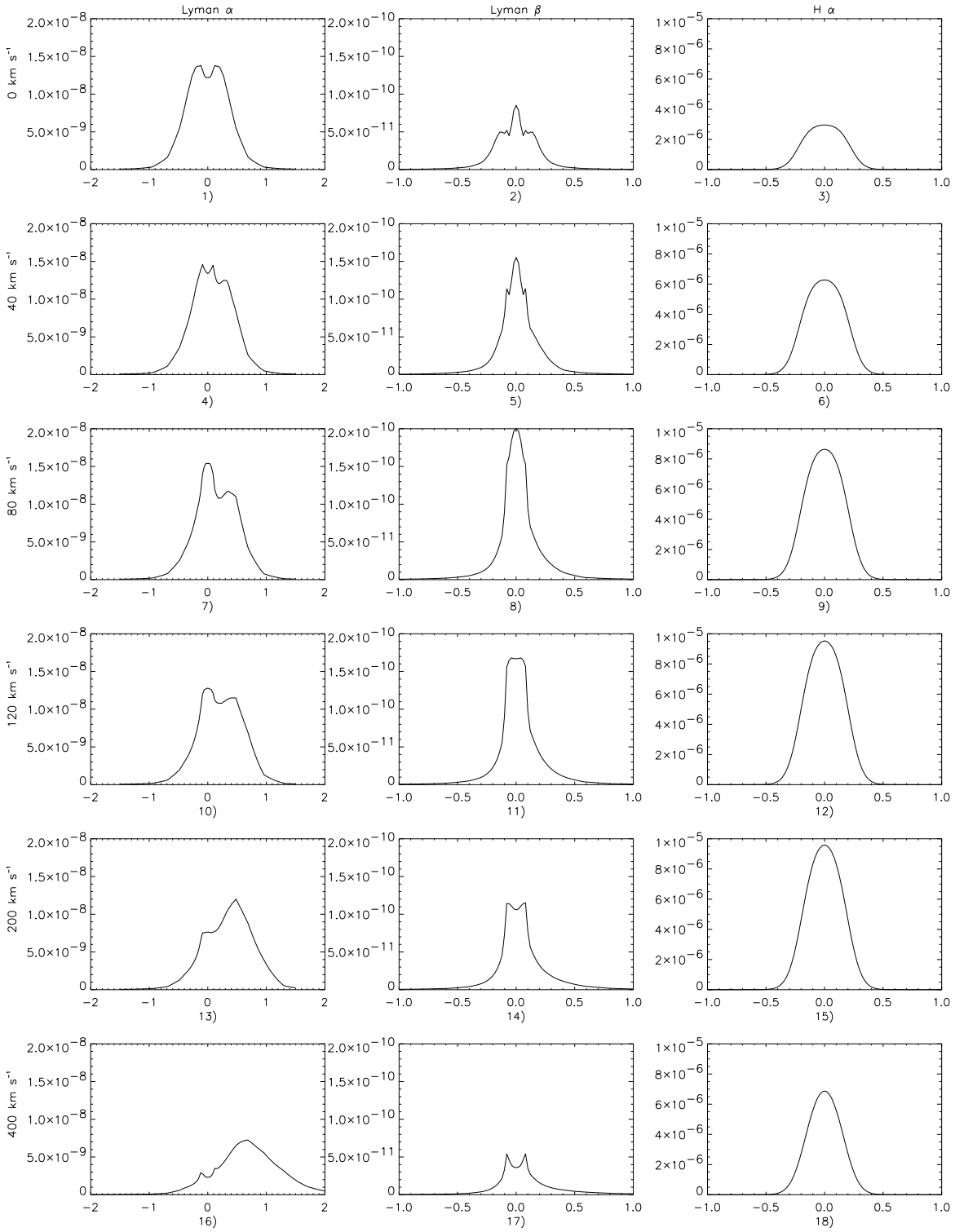

Fig. 4. The profiles of Lα, Lβ, and Hα (columns 1, 2, 3) for 0, 40, 80, 120, 200 and 400 km s^{-1}. The temperature is 4300 K and the width 2 000 km. The intensity is in erg s^{-1}cm^{-2}sr^{-1}Hz^{-1} and the wavelength in Å.

the redshift, the blue peak of the incident profile is absorbed at the center of the line. The incident photons corresponding to the blue peak are scattered in a non-coherent way and in combination with the high opacity are responsible for the double peak. The red peak of the incident profile is scattered coherently in the red wing and forms the red peak of the emergent profile. For velocities higher than 120 km s^{-1}, the emergent profile contains a bright feature in the red wing only (Fig. 4.13, 4.16). The incident profile, which has a single peak structure (Fig. 1) is quasi-coherently scattered in the red wing of the line. The opacity in the blue wing is not sufficient for the creation of a blue peak as in the case discussed in the last section (Fig. 2.7) where the temperature was 8 000 K.

For low velocities and temperature, the Lβ line presents a central peak (Fig 4.2, 4.5, 4.8). This structure is surrounded by two small symmetric peaks caused by the high opacity. For $\Delta\lambda \geq 0.2$ we see the red enhancement due to the velocity effect. For $v \geq 120\,\mathrm{km\,s^{-1}}$ the central peak disappears and the Lβ profile is reversed (Fig. 4.11, 4.14, 4.17). The absorbed Lβ photons can be reemitted as Hα photons and then can escape from the medium due to the low Hα opacity (HGV). At low velocity this mechanism reduces the Lβ radiative field and the emergent Lβ line is lower than the incident one. For the same reason, the Lβ radiation field is higher near the surface than in the interior. This fact explains the central peak of the emergent profile. With the increasing velocity, the $2 \rightarrow 3 \rightarrow 1$ transition enhances the Lβ radiation field because of the brightening of the Hα line. When the velocity $v \gtrsim 120\,\mathrm{km\,s^{-1}}$, the center of the absorption profile scatters the incident photons coming from the (faint) blue wing of the redshifted incident Lβ profile. The result is that the emergent Lβ line is reversed. The low amount of thermal emission allows stronger velocity effects in Lβ as compared with the 8 000 K case. But the asymmetries are always lower than the Lα ones because of the coupling with Hα.

At 15 000 K and with the thickness fixed at 2 000 km, the emergent Lα and Lβ present symmetric reversed profiles for all velocities (Fig. 5 columns 1 and 2). However some asymmetries exist in the wings and can be shown in a semi-logarithmic scale.

We find that, as the temperature increases, the asymmetries become less visible in the profiles. We present, in Table 1 the optical depth, the maximum intensity, and the intensity in the red wing at 1 Å from line center for Lα and Lβ for three values of the temperature. The intensities are in erg s^{-1}cm^{-2}sr^{-1}Hz^{-1}. We show the intensity at 1 Å because at this wavelength the scattering is quasi-coherent and the velocity signature is obvious. We fix the velocity to 200 km s^{-1}. At this velocity the peak of the incident Lα profile has an intensity of $I_{inc} = 1.5 \times 10^{-8}$erg s^{-1}cm^{-2}sr^{-1}Hz^{-1}. For T=4300 K the emergent Lα profile is less intense than the incident one. The incident photons dominate the radiative transfer and so the velocity effects are very visible on the emergent profile. At 15 000 K the emergent profile is 20 times brighter than the incident one because of the enhancement of the thermal excitation of Lα, so the asymmetry of the profile is weaker than at 4300 K (at least by a factor of 20). But the enhancement of temperature increases the ionization and decreases the opacity of the Lyman lines; as a result the wings, where the photons undergo coherent scattering are lower. The Hα line has a quasi-gaussian profile (Fig. 4 and 5, third column). With increasing temperature, the full width at half maximum (FWHM) increases because of the Doppler broadering while the intensity decreases because of the ionization.

The increase of the slab width broadens the Lyman line profiles but does not change much their general asymmetries (Fig. 6.1, 6.2 for Lα and 6.3, 6.4 for Lβ). It has an opposite effect on the Lyman lines than the temperature, because it increases the optical thickness. The ionization decreases the opacity and consequently the FWHM, in contrast to the geometrical width which enhances it.

The Hα profile is broader and more intense because of the enhancement of opacity. For a slab of 10 000 km, the core of the line is optically thick and the profile shows a saturation of the intensity at the center of the line (Fig. 6.5, 6.6). But at 15 000 K the ionization reduces the opacity and the Hα has a quasi-gaussian profile (Fig. 6.5, 6.6).

The increase of the pressure (Fig. 7) enhances the amount of scattering processes in the wings of the Lyman lines while the line core is saturated by the strong opacity. So the pressure increases the wing asymmetry in the same way the slab width does (Fig. 7, columns 1 and 2). In the Hα line (Fig. 7, third column) the core saturation is present only for 1 dyn cm^{-2}.

5. The emission measure

The emission measure, $EM = \int N_e^2\, dl$ can be used to derive the electron density and the filling factor in a structure. GHV presented the correlation between the total intensity in the Hα line and the emission measure for static structures. The effect of the velocity on the emission measure was discussed by Schmieder et al. (1995) in the context of post-flare loops. We now introduce this effect into our modelling.

The variations of velocity changes the relation between Hα and the emission measure because of the brightening in Hα (compare solid and broken lines in Fig. 8).

Let us begin with the evolution of the emission measure with the velocity for a given prominence model. As an example, in Fig. 8, the family of points situated at $\sim 5 \times 10^{28}\,\mathrm{cm^{-5}}$ corresponds to a model of 4300 K, 2 000 km, and 0.1 dyn cm^{-2} (they are represented with squares in Fig. 8). This group shows that when the velocity is higher than 120 km s^{-1} the emission measure decreases. The same behavior is observed for all models with temperatures of 4300 K and 8 000 K, except for those with a width of 10 000 km where the decrease of the emission measure is smaller. The emission measure of models having a temperature of 15 000 K is independent of the velocity. For the two lower values of the temperature, the behaviour of emission measure can be explained by the photoionization due to the Lyman and the Balmer continua. The Lyman and Balmer photoionization terms are described by the equation (2).

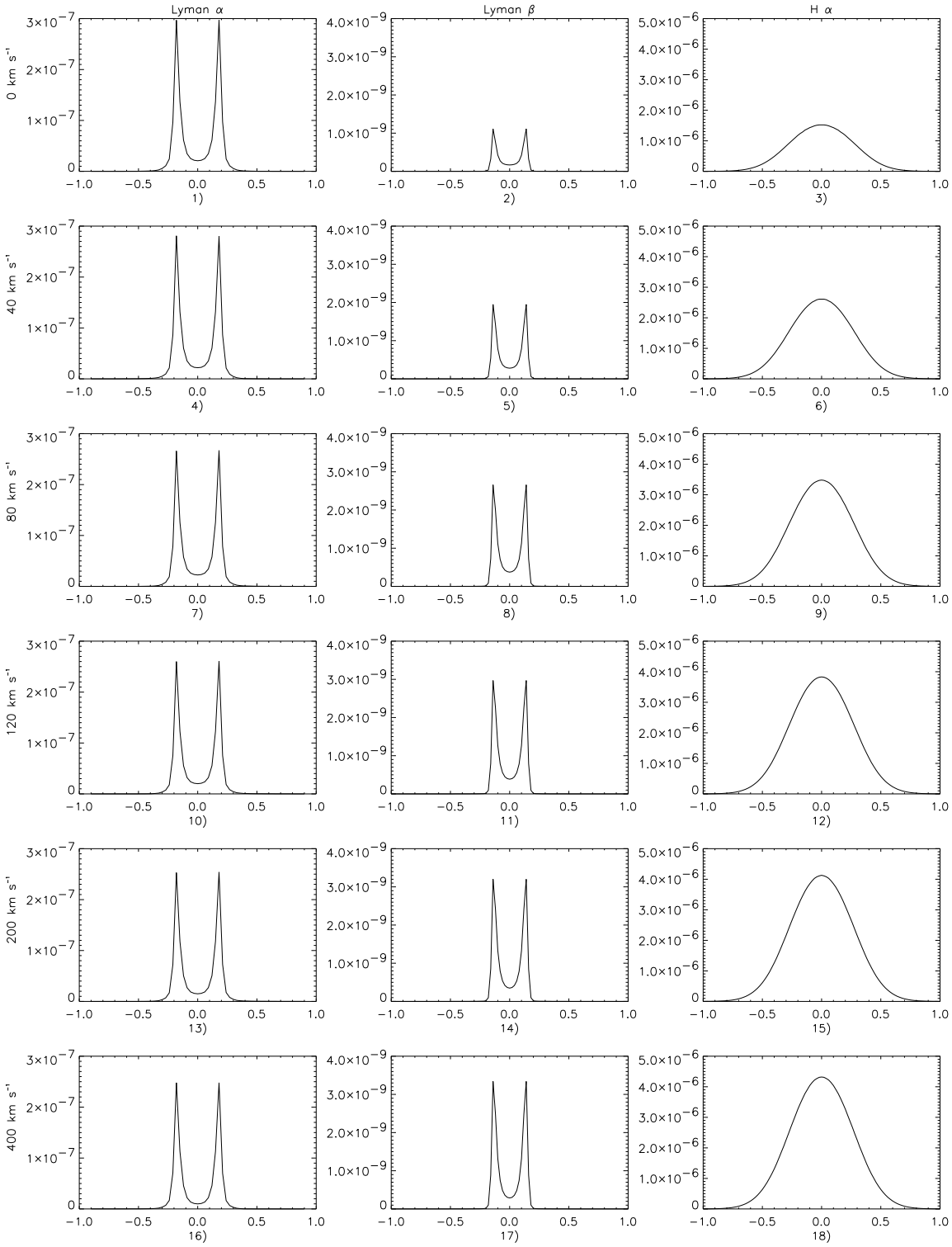

Fig. 5. The same as in Fig. 4 but for a temperature of 15 000 K.

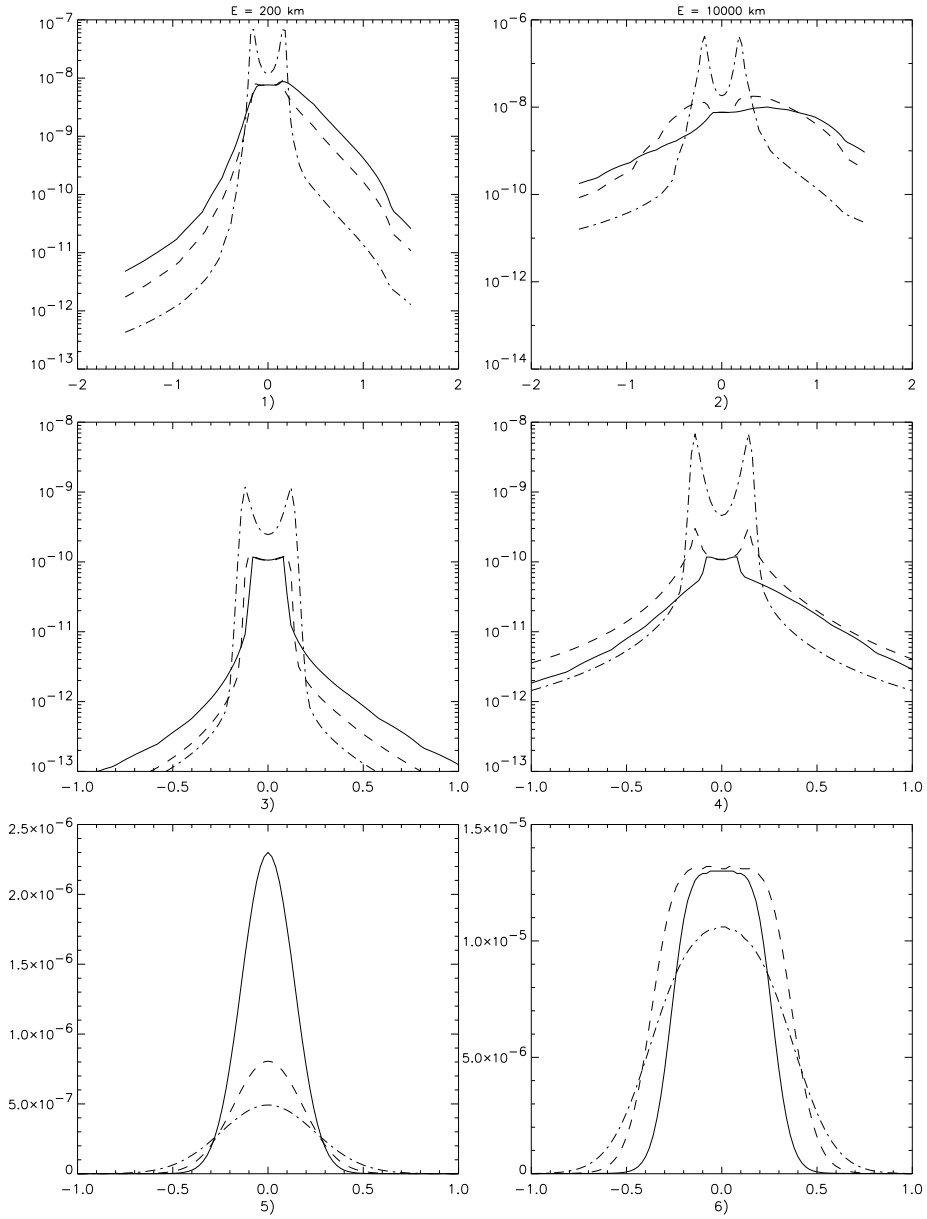

Fig. 6. The effect of the slab width on lines profiles. Lα, Lβ and Hα are in the first, second and third rows respectively. The first column is taken from a model with a width D=200 km, and the second one from a model with D=10 000 km. The velocity of the structure in all cases is of 200 km s^{-1} (dashes are for T = 4300 K, full line for T = 8 000 K and dash-dots for T = 15 000 K).

$$N_{jc} = 4\pi N_j \int_{\nu_0}^{+\infty} k_\nu \frac{J_\nu}{h\nu} d\nu \qquad (2)$$

Here, j denotes the bound level, ν_0 is the frequency at the continuum threshold, k_ν is the atomic absorption coefficient and J_ν is the mean intensity. N_{jc} is expressed in cm^{-3} s^{-1}. The two photoionization terms are of the same order of magnitude.

As the velocity increases, the dimming effect in Lα reduces the N_2 population and increases marginally the N_1 one (Fig. 3.a, 3.b of GVG). The Balmer continuum is optically thin ($\tau_{2c} \simeq 10^{-5}$), so the only dependence of the Balmer photoionization with velocity comes from N_2. The decrease of N_{2c} induces the decrease of N_e observed in the emission measure.

As the Lyman continuum is optically thick ($\tau \sim 40$) the J_ν in equation (2) is dominated by the photons created inside the prominence by recombination.The intrinsic source function is described as $S_{int} \sim \frac{N_e^2}{N_1}$. The result is that N_{1c} is reduced because of the decrease of the electron density at high velocities (and the slight increase of N_1).

In the case of high temperatures the thermal effects dominate the radiative ionization so, the emission measure does not depend on the velocity, thermal effects are important in the case of high thickness as well.

6. Discussion and conclusion

We have studied the effect of mass motion on the radiative transfer in a prominence. This could be mass flows inside an active prominence or the outward velocity of the prominence during an eruption.

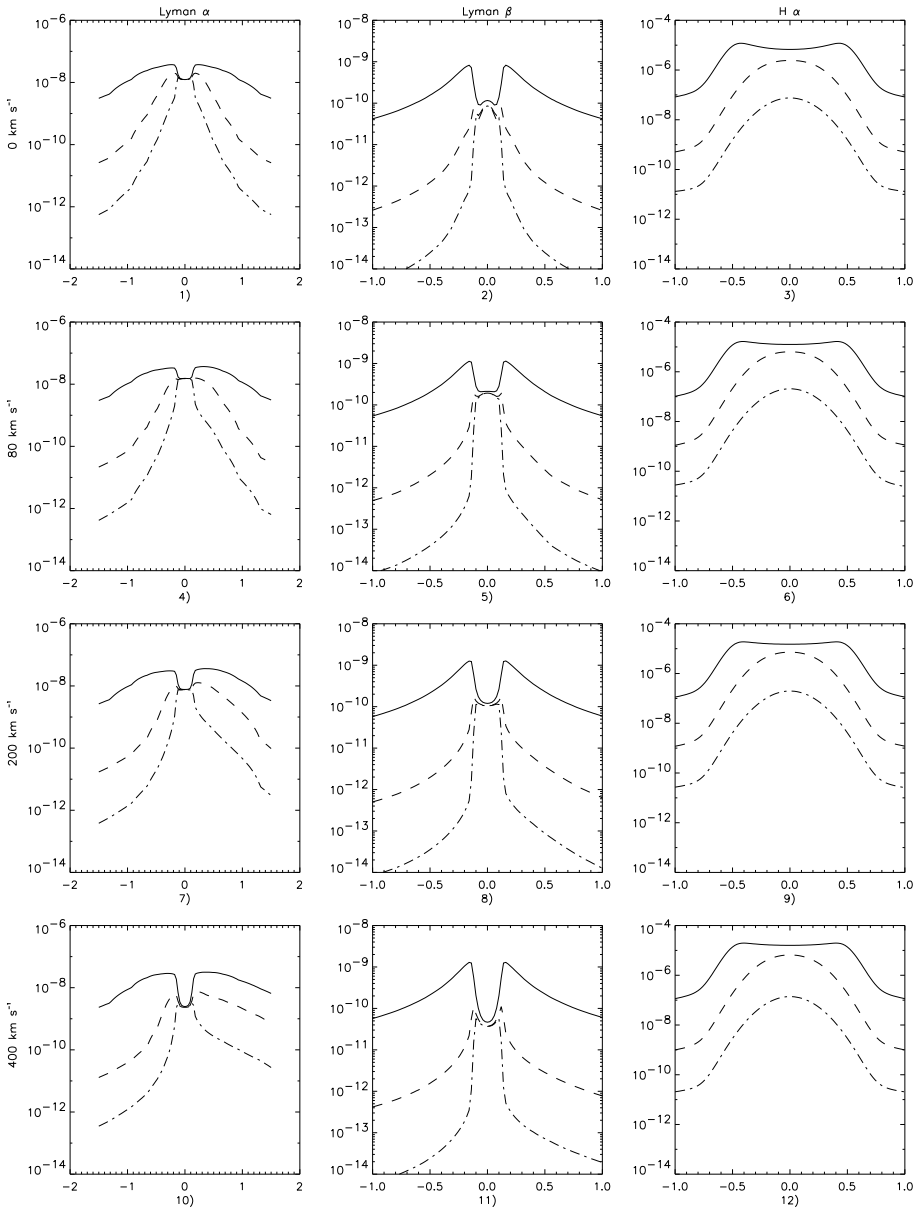

Fig. 7. The effect of the plasma pressure on lines profiles. Lα, Lβ and Hα are in the first, second and third columns respectively. The velocities are 0, 80, 200 and 400 km s^{-1} (rows 1, 2, 3 and 4). Full line is for P = 1 dyn cm^{-2}, dashes for 0.1 and dot-dashes for 0.01 dyn cm^{-2}. The temperature is 8 000 K and the width 2 000 km.

When we use PRD for the treatment of resonance scattering, we find that the Lα and Lβ profiles are very sensitive to the presence of mass motions. But this behavior depends on the thermodynamic condition inside the prominence. For typical temperatures in quiescent prominences (Tandberg-Hanssen 1995) we see that the two first lines of the Lyman series, and especially Lα, depend strongly on mass motions. In the case of 15 000 K, a value measured in eruptive prominences (Poland and Munro 1976), the profiles are always symmetric. The Lβ and Hα intensities increase with the velocity up to about 120 km s^{-1}. The width of the structure along the line of sight introduces an other dependence of the profiles through the optical thickness. Indeed the total intensity is a function of the velocity for any value of temperature that we studied except for high velocities in the case of a temperature of 15 000 K (GVG and Fig. 5). We have also confirmed that the correlation between the Hα and the emission measure, proposed by GHV as a diagnostic tool, is under the influence of radial velocities.

Of course, the representation of the prominence geometry by a finite 1D slab can be improved with numerical tools solving the radiative transfer in two dimensions (Paletou, 1996). The 2D representation will allow a stronger penetration of the incident radiation from bellow. This should increase the effect of radial velocities, especially for Hα and consequently Lβ lines.

In a next paper we will discuss the early evolution of the prominence eruption phenomenon. We plan to use our radiative calculation tool in combination with models describing the prominence eruption. With models giving the temperature, the pressure, the altitude, and the geometry of the erupted material in function of time, we shall be able to compute the varying hydrogen spectrum as a function of time and to compare these calculations with observations of eruptive prominences.

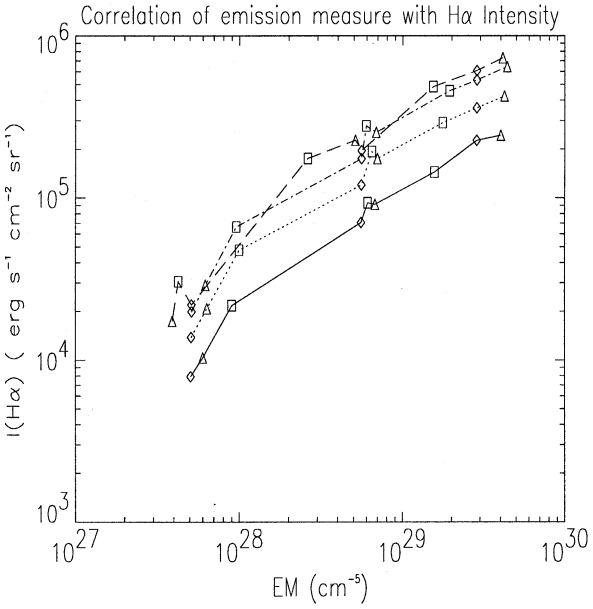

Fig. 8. The emission measure as a function of the Hα integrated intensity for different prominence models with different velocities. The symbols indicate the different temperatures and the different line-styles the value of the velocity. Squares :4300 K, triangles :8 000 K, diamonds :15 000 K. Solid line is for 0 km s^{-1}, dots for 40 km s^{-1}, dash dots for 120 km s^{-1}, and long dashes for 400 km s^{-1}. The prominence models for which the emission measure is near 10^{28}cm^{-5} correspond to a geometrical thickness of 200 km. The ones around 10^{29} cm^{-5} to 2 000 km and the ones with values of the order of 4×10^{29} cm^{-5} to a thickness of 10 000 km.

Using the Lα, Lβ and Hα profiles and total intensities we can diagnose the radial velocities present in prominences. This tool can be applied to observations obtained with SUMER and UVCS for the hydrogen Lyman lines. Other instruments such as EIT and CDS will allow the observation of lines from other species (Fleck et al. 1995).

With complementary line-of-sight measurements of Doppler shifts, it will be possible to determine the full velocity vectors. We plan to observe eruptive prominences using a dedicated Joint Observing Program (JOP4).

Acknowledgements. The authors thank Dr. Petr Heinzel for many corrections and discussions which helped to improve the paper. All the above radiative transfer computations have been made with a computer allocation on the Cray 98 of the "Institut du Developpement et des Ressources en Informatique Scientifique".

References

Auer L. H. and Mihalas D., 1970, MNRAS, 149, 65
David K. H., 1961, Z., Astrophys., 53, 37
Fleck B., Domingo V. and Poland A. I.(eds.)"The SOHO Mission", 1995, 162, 1-2
Gontikakis C., Vial J.-C. and Gouttebroze P., 1996, Solar Phys. (in press) (GVG)
Gouttebroze P., Heinzel P. and Vial J.-C., 1993, A&A, 99, 513 (GHV)
Heinzel P., Bommier V. and Vial J.-C., 1996, Solar Phys., 164, 211
Heinzel P., Gouttebroze P. and Vial J.-C., 1987, A&A, 183, 351 (HGV)
Heinzel P. and Rompolt B., 1987, Solar Phys., 110, 171(HR)
Hirayama T., 1963, PASJ, 15, 122
Hummer D. G., 1962, MNRAS, 125, 21
Hyder C. and Lites B., 1970, Solar Phys., 14, 147
Milkey R. W., Heasley J. N., Schmahl E. J. and Engvold O., 1978, in IAU Colloquium 44, Physics of Solar Prominences, ed. Jensen E., Maltby P. and Orral F. Q. (Dordrecht:Reidel), p. 53.
Paletou F., Vial J.-C. and Auer L., 1993, A&A, 274, 571
Pierce A. K. and Slaughter C. D., 1977, Solar Phys., 51, 25
Pierce A. K., Slaughter C. D. and Weinberger D., 1977, Solar Phys., 52, 179
Rompolt B., 1967a, Acta Astron. 17, 329.
Rompolt B., 1967b, Acta Universitatis Wratislaviensis, No 75.
Rompolt B., 1969, Acta Universitatis Wratislaviensis, No 77, 117.
Schmieder B., Heinzel P., Wiik J. E., Lemen J., Anwar B., Kotrč P. and Hiei E., 1995, Solar Phys., 156, 337
Vial J.-C., 1982, Ap. J., 253, 330
Zelenka A., 1976, A&A, 48, 75
Tandberg-Hanssen E., 1995, The Nature of Solar Prominences, Kluwer Academic Publishers

This article was processed by the author using Springer-Verlag LaTeX A&A style file *L-AA* version 3.